

# Possible Superconductivity in Electron-doped Chromium Pnictide LaOCrAs

Wan-Sheng Wang,<sup>1</sup> Miao Gao,<sup>1</sup> Yang Yang,<sup>2</sup> Yuan-Yuan Xiang,<sup>3</sup> and Qiang-Hua Wang<sup>4,5</sup>

<sup>1</sup>*Department of Physics, Ningbo University, Ningbo 315211, China\**

<sup>2</sup>*College of Physics and Electronic Engineering, Zhengzhou University of Light Industry, Zhengzhou 450002, China*

<sup>3</sup>*College of Science, Hohai University, Nanjing, 210098, China*

<sup>4</sup>*National Laboratory of Solid State Microstructures and School of Physics, Nanjing University, Nanjing, 210093, China*

<sup>5</sup>*Collaborative Innovation Center of Advanced Microstructures, Nanjing University, Nanjing, 210093, China†*

We constructed an effective tight-binding model with five Cr 3d orbitals for LaOCrAs according to first-principles calculations. Basing on this model, we investigated possible superconductivity induced by correlations in doped LaOCrAs using the functional renormalization group (FRG). We find that there are two domes of superconductivity in electron-doped LaOCrAs. With increasing electron doping, the ground state of the system evolves from G-type antiferromagnetism in the parent compound to an incipient  $s_{\pm}$ -wave superconducting phase dominated by electron bands derived from the  $d_{3z^2-r^2}$  orbital as the filling is above 4.2 electrons per site on the  $d$ -orbitals of Cr. The gap function has strong octet anisotropy on the Fermi pocket around the zone center and diminishes on the other pockets. In electron over-doped LaOCrAs, the system develops  $d_{x^2-y^2}$ -wave superconducting phase and the active band derives from the  $d_{xy}$  orbital. Inbetween the two superconducting domes, a time-reversal symmetry breaking  $s + id$  SC phase is likely to occur. We also find  $s_{\pm}$ -wave superconducting phase in the hole-doped case.

PACS numbers: 74.20.-z, 71.27.+a, 74.20.Rp

## I. INTRODUCTION

Transition metal pnictides have received much attention since the discovery of high- $T_c$  superconductivity in F-doped LaOFeAs.<sup>1</sup> Along with the extensively studied iron pnictides, some iron-free isostructural compounds have been found to be superconductors, such as pnictides based on Ni, Rh, Ir, Pt, and Pd, etc.<sup>2–14</sup> However, Mn-based pnictides are antiferromagnetic (AFM) insulators.<sup>15–21</sup> No superconductivity has been found when the antiferromagnetism is suppressed by pressure in LaOMnP<sup>22</sup> or by high electron doping through H<sup>−</sup> substitution of O<sup>2−</sup> in LaOMnAs.<sup>23</sup> It is likely because the strong Hund's rule coupling in the half-filled  $d^5$  configuration forces the Mn-ion to form a high-spin state that is always toxic to superconductivity. With the  $d^5$  configuration as the reference, it would be interesting to look for superconductivity in compounds with  $d^4$  configuration, such as in the isostructural chromium pnictides, which mirrors the  $d^6$  configuration in parent iron pnictides.<sup>24,25</sup> This motivation makes better sense after the observation of superconductivity in CrAs (under high pressures)<sup>26,27</sup> and  $A_2\text{Cr}_3\text{As}_3$  ( $A = \text{K, Rb, Cs}$ ) under ambient pressure.<sup>28–30</sup>

In fact,  $\text{BaCr}_2\text{As}_2$  and  $\text{SrCr}_2\text{As}_2$  were synthesized in 1980,<sup>31</sup> and the physical properties and electronic structure of  $\text{BaCr}_2\text{As}_2$  were investigated<sup>32</sup> after the discovery of superconductivity in doped  $\text{BaFe}_2\text{As}_2$ .<sup>33</sup> The results show that  $\text{BaCr}_2\text{As}_2$  is an AFM metal, with a G-type order and very strong magnetic interactions. In addition, an analogous compound  $\text{EuCr}_2\text{As}_2$  with similar electronic properties were reported.<sup>34</sup> A series of  $\text{LnOCrAs}$  ( $\text{Ln} = \text{La, Ce, Pr, and Nd}$ ) compounds were synthesized by Park *et al.*<sup>35</sup> All the members show metallic electronic conduction, and LaOCrAs is ordered in G-type

antiferromagnetism with a large spin moment of  $1.57\mu_B$  along the  $c$  axis revealed by powder neutron diffraction under 300K. Recently, a new chromium oxypnictide  $\text{Sr}_2\text{Cr}_3\text{As}_2\text{O}_2$  containing  $\text{CrO}_2$  and  $\text{Cr}_2\text{As}_2$  square-planar lattices were reported. It is also an AFM metal with a G-type AFM order in the  $\text{Cr}_2\text{As}_2$  plane under 291K.<sup>36</sup> However, superconductivity has not yet been observed in any of the above parent  $\text{Cr}_2\text{As}_2$ -layer based materials. But as in the case of iron pnictides, superconductivity may appear upon doping the parent compounds to a sufficient level.

In this work, we investigate possible superconductivity in doped chromium pnictide LaOCrAs. First, we calculate the electronic structure of LaOCrAs by first-principles calculations and construct an effective five-orbital tight-binding model. Second, on the basis of the tight-binding model, we investigate possible superconductivity induced by correlations in doped LaOCrAs using the unbiased singular-mode functional renormalization group (SMFRG).<sup>37–45</sup> In the parent compound, we confirm the G-type antiferromagnetism found in experiments. Upon electron doping, We find that there are two domes of superconductivity as the filling is above 4.2 electrons per site (henceforth on the  $d$ -orbitals of Cr). The first superconducting phase has an incipient  $s_{\pm}$ -wave pairing symmetry, with gap sign change on the electron Fermi pockets and the virtual hole pockets. The gap function has octet anisotropy on the Fermi pocket around the zone center, and diminishes on the other pockets. This superconducting phase is triggered by spin fluctuations between the Fermi pockets around  $\Gamma$  and  $M$  points in the unfolded Brillouin Zone (BZ), where the orbital contents of the Bloch states are dominant by  $d_{3z^2-r^2}$ . With further electron doping, the system develops  $d_{x^2-y^2}$ -wave superconducting phase, which is related

to spin fluctuations between the Fermi pockets around  $X$  and  $Y$  points, where the orbital characters are dominant by  $d_{xy}$ . Inbetween the two superconducting phases, a time-reversal-symmetry breaking  $s + id$  phase would be energetically favorable. In the hole doped case we find  $s_{\pm}$ -wave superconductivity is favorable.

The rest of the paper is organised as follows. In Sec.II, we construct an effective model for LaOCrAs through first-principles calculations and briefly introduce the SM-FRG method. In Sec.III, we discuss the results for doped LaOCrAs and conclude by a phase diagram. Finally, a summary and experimental perspectives are discussed in Sec.IV.

## II. MODEL AND METHOD

LaOCrAs has a ZrCuSiAs-type structure with the space group  $P4/nmm$  (No. 129). Because of the tetrahedral coordination of As, there are two Cr atoms per unit cell. The experimentally determined lattice constants are  $a = 4.04123\text{\AA}$  and  $c = 8.98637\text{\AA}$ . We obtain the band structure by the Quantum-ESPRESSO package,<sup>46</sup> and then construct the maximally localized Wannier functions.<sup>47</sup> These maximally localized Wannier functions are centered at two Cr sites in the unit cell, transforming as  $d_{3z^2-r^2}$ ,  $d_{xz}$ ,  $d_{yz}$ ,  $d_{xy}$ , and  $d_{x^2-y^2}$ , where  $X$ ,  $Y$ ,  $Z$  refer to the axes of the large unit cell. Since the two Cr atoms satisfy the group symmetry, we further unfold the BZ with one Cr atom per small unit cell and construct a five-orbital model. For convenience, we rotate the crystal coordinates axes and the orbitals basis by  $\pi/4$ , from  $X$ - $Y$  to  $x$ - $y$ .<sup>48</sup> Since the inter-layer coupling is weak, we only consider the in-plane hopping for brevity. The in-plane hopping integrals  $t_{\Delta_x, \Delta_y}^{\mu, \nu}$  are displayed in Table.I, where  $[\Delta_x, \Delta_y]$  denote the in-plane hopping vector, and  $\mu, \nu$  label the five rotated  $d$ -orbitals:  $d_{3z^2-r^2}$ ,  $d_{xz}$ ,  $d_{yz}$ ,  $d_{x^2-y^2}$ , and  $d_{xy}$ . They are directed along the nearest Cr-Cr bonds.

We obtain the band structure in the unfolded BZ as shown in Fig.1(a). The bands close to Fermi level around  $\Gamma$  and  $M$  points are nearly flat, resulting in large density of states (DOS) near Fermi level, as shown in the Fig.1(b), where the DOS has two peaks around the Fermi level. The large DOS near Fermi level makes the system particularly susceptible to various instabilities driven by electron correlations, as will be discussed later. Slightly above the two peaks, there is also a peak in DOS due to the van Hove singularities in the third band. Figs.2(a)-(d) show the Fermi surface (FS) of LaOCrAs encoded with the spectral weights in  $d_{3z^2-r^2}$ ,  $d_{xz}$ ,  $d_{x^2-y^2}$ , and  $d_{xy}$  components. The  $d_{yz}$  weight is not shown since it is equivalent to that of  $d_{xz}$  upon a rotation of  $\pi/2$ . We see that the  $\alpha$  and  $\gamma$  pockets are dominant by  $d_{3z^2-r^2}$  orbital, and in particular the weight has octet-wise deep minima on  $\alpha$ . The  $\beta$  pockets are dominant by  $d_{xy}$  orbital, and finally the  $\delta$  pockets by  $d_{3z^2-r^2}$  and  $d_{xy}$  orbitals.

We consider the following local interactions on Cr

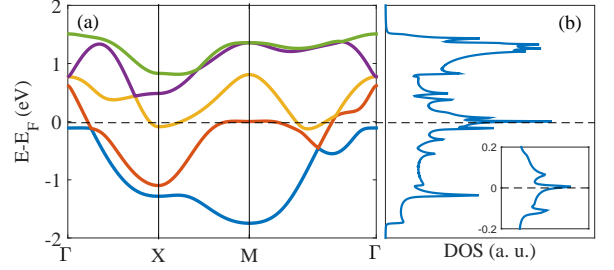


FIG. 1: (Color online) (a) Band structure of LaOCrAs based on the five-band model in the unfolded Brillouin zone. (b) The corresponding density of states. Inset shows the enlarged window near Fermi level.

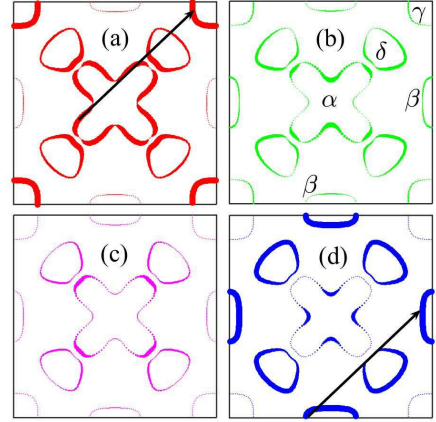


FIG. 2: (Color online) Fermi surface (FS) of LaOCrAs in the unfolded Brillouin zone. From (a)-(d) the width of each FS line is proportional to its spectral weights in  $d_{3z^2-r^2}$ ,  $d_{xz}$ ,  $d_{x^2-y^2}$ , and  $d_{xy}$  components. The arrows in (a) and (d) denote two types of scattering with momentum  $\mathbf{Q}$  around  $(\pi, \pi)$ . The  $\alpha$ ,  $\beta$ , and  $\gamma$  in (b) denote the Fermi pockets around  $\Gamma$ ,  $X$ (or  $Y$ ), and  $M$  points, respectively. The pockets around the middle points of  $\Gamma$ - $M$  lines are denoted by  $\delta$ .

atoms:

$$\begin{aligned}
 H_I &= U \sum_{i\mu} n_{i\mu\uparrow} n_{i\mu\downarrow} + U' \sum_{i, \mu > \nu} n_{i, \mu} n_{i, \nu} \\
 &+ J_H \sum_{i, \mu > \nu, \sigma \sigma'} c_{i\mu\sigma}^\dagger c_{i\nu\sigma'} c_{i\nu\sigma}^\dagger c_{i\mu\sigma'} \\
 &+ J'_H \sum_{i, \mu \neq \nu} c_{i\mu\uparrow}^\dagger c_{i\mu\downarrow}^\dagger c_{i\nu\downarrow} c_{i\nu\uparrow},
 \end{aligned} \tag{1}$$

where  $i$  denotes Cr sites,  $\sigma$  is the spin polarity,  $\mu$  and  $\nu$  denote five Cr  $3d$  orbitals,  $n_{i\mu} = \sum_{\sigma} c_{i\mu\sigma}^\dagger c_{i\mu\sigma}$ ,  $U$  is the intra-orbital repulsion,  $U'$  is the inter-orbital repulsion,  $J_H$  is Hund's rule coupling, and  $J'_H$  is the pair hopping term, and we use the Kanamori relations  $U' = U - 2J_H$  and  $J_H = J'_H$  so that we are left with two independent interaction parameters ( $U, J_H$ ). The interactions can lead to competing collective fluctuations in density-wave and

TABLE I: Hopping integrals  $t_{\Delta_x, \Delta_y}^{\mu, \nu}$  (in units of eV) for effective five Cr 3d bands model.  $[\Delta_x, \Delta_y]$  denotes the in-plane hopping vector, and  $(\mu, \nu)$  the orbitals.  $\sigma_y$ ,  $I$  and  $\sigma_d$  are three basic group operation, corresponding to  $t_{-\Delta_x, \Delta_y}^{\mu, \nu}$ ,  $t_{-\Delta_x, -\Delta_y}^{\mu, \nu}$ , and  $t_{\Delta_y, \Delta_x}^{\mu, \nu}$ , respectively. Notice that the  $x$  and  $y$  axes are along the nearest Cr-Cr bond. The basis of the orbitals are also along the nearest Cr-Cr bond. The order of the five orbitals are:  $(d_{3z^2-r^2}, d_{xz}, d_{yz}, d_{x^2-y^2}, d_{xy})$ , with the corresponding on-site energies (11.513, 11.795, 11.795, 11.455, 11.967) eV, respectively. The chemical potential is 11.486 eV.

$(\mu, \nu) \backslash (\Delta_x, \Delta_y)$	(1, 0)	(1, 1)	(2, 0)	(2, 1)	(2, 2)	$\sigma_y$	$I$	$\sigma_d$
(1, 1)	-0.012	0.037	-0.048	-0.001	-0.009	+	+	+
(1, 2)	-0.095	0.076	0.012	0.013	0.008	-	-	(1,3)
(1, 3)		0.076		0.022	0.008	+	-	(1,2)
(1, 4)	-0.263		-0.038	-0.014		+	+	-
(1, 5)		-0.104		-0.005	0.003	-	+	+
(2, 2)	-0.300	0.183	-0.018	0.013	0.014	+	+	(3,3)
(2, 3)		0.047		0.016	0.006	-	+	+
(2, 4)	-0.299	0.078	-0.017	-0.012	-0.001	-	-	-(3,4)
(2, 5)		0.055		0.010	-0.003	+	-	(3,5)
(3, 3)	0.122	0.183	0.002	0.003	0.014	+	+	(2,2)
(3, 4)		-0.078		-0.012	0.001	+	-	-(2,4)
(3, 5)	0.257	0.055	0.023	0.019	-0.003	-	-	(2,5)
(4, 4)	0.415	-0.025	-0.007	-0.004	0.010	+	+	+
(4, 5)				-0.017		-	+	-
(5, 5)	0.036	0.100	-0.012	-0.030	-0.030	+	+	+

pairing channels, which we handle by SMFRG as follows. A general interaction vertex function can be decomposed as scattering matrices between composite bosons,

$$V_{\mathbf{k}, \mathbf{k}', \mathbf{q}}^{\mu, \nu; \lambda, \eta} \rightarrow \sum_m S_m(\mathbf{q}) \phi_m^{\mu, \nu}(\mathbf{k}, \mathbf{q}) [\phi_m^{\lambda, \eta}(\mathbf{k}', \mathbf{q})]^*, \quad (2)$$

either in the superconducting (SC), spin-density wave (SDW), or charge-density wave (CDW) channels. Here,  $(\mu, \nu, \lambda, \eta)$  are orbital indices,  $\mathbf{q}$  is the collective momentum, and  $\mathbf{k}$  (or  $\mathbf{k}'$ ) is an internal momentum of the Fermion bilinears  $c_{\mathbf{k}+\mathbf{q}, \mu}^\dagger c_{-\mathbf{k}, \nu}^\dagger$  and  $c_{\mathbf{k}+\mathbf{q}, \mu}^\dagger c_{\mathbf{k}, \nu}$  in the particle-particle and particle-hole channels, respectively. In the following we define, in a specific channel,  $S(\mathbf{q})$  as the leading attractive eigenvalue at  $\mathbf{q}$ , and  $S$  as the globally leading one. The SM-FRG provides the *coupled* flow of all channels versus a decreasing energy scale  $\Lambda$  (the infrared limit of the Matsubara frequency in our case). The fastest growing eigenvalue  $S(\mathbf{Q})$  implies an emerging order associated with a collective wave vector  $\mathbf{Q}$  and an eigenfunction (or form factor)  $\phi(\mathbf{k}, \mathbf{Q})$ . (Notice that  $\mathbf{Q} = 0$  in the SC channel because of the Copper instability, but may evolve with  $\Lambda$  in the other channels.) The divergence scale provides an upper limit of the ordering temperature. More technical details can be found elsewhere.<sup>37-45</sup>

### III. RESULTS AND DISCUSSION

We first discuss the electron-doped case at band filling  $n = 4.24$ , with the Fermi level slightly above the flat band around the  $M$  point. The  $\gamma$  pocket is absent here as shown in Fig.3(b), but we should emphasize that our SM-FRG includes virtual excitations from all bands. Fig.3(a)

shows the FRG flow of the leading eigenvalues  $S_{SC, SDW}$  versus the running energy scale  $\Lambda$  for  $U = 1.0\text{eV}$  and  $J_H = U/4$ . Since the CDW channel remains weak during the flow, we shall not discuss it henceforth. We find that the SDW channel is enhanced in the intermediate stage, but saturate at low energy scales because of lack of phase space for low-energy particle-hole excitations. The momentum  $\mathbf{q}$  associated with the leading  $S_{SDW}$  is around  $(\pi, \pi)$  at high energy scales and only changes slightly during the flow. The inset of Fig.3(a) shows  $S_{SDW}(\mathbf{q})$  versus  $\mathbf{q}$  at the final stage. There are peaks around  $\mathbf{Q} = (\pi, \pi)$ . We checked that the associated form factors describe site-local spins, indicating G-type AFM fluctuations, consistent with the G-type AFM order in the parent compound.<sup>35</sup> This G-type spin fluctuations can be associated with two types of scattering as shown in Fig.2.

The enhancement of  $S_{SDW}$  in the intermediate stage triggers attractive pairing interaction  $S_{SC}$  to increase, and the latter diverges eventually on its own via the Copper mechanism. Thus, the system develops an SC instability at the divergence energy scale as shown in Fig.3(a). Since the gap functions of the singlet SC state would change sign on the two  $\mathbf{k}$  points connected by the spin fluctuation vector  $\mathbf{Q}$ , there are two competing pairing states: (i) Incipient  $s_{\pm}$ -wave, with sign change of the gap function on the  $\alpha$  and  $\gamma$  pockets. (Note the  $\gamma$  pocket is slightly below the Fermi level here.) (ii)  $d_{x^2-y^2}$ -wave, with sign change on the two  $\beta$  pockets. By checking the pairing form factor (see the Appendix A for details) we find the incipient  $s_{\pm}$ -wave is realized at the present doping level.<sup>49</sup> The gap function in the band basis (see Appendix A) is shown along the Fermi surfaces in Fig.3(b). We observe that the gap function on the  $\alpha$  pocket has octet-wise deep minima, and the amplitude

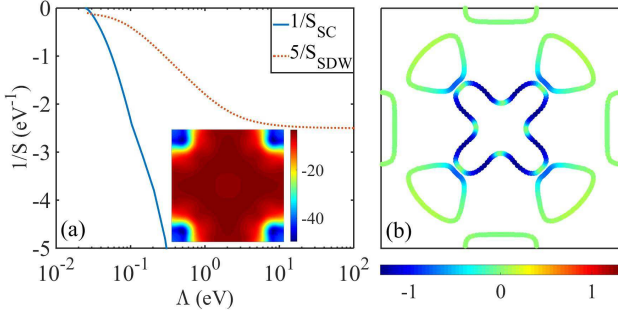


FIG. 3: (Color online) Results for  $n = 4.24$  with  $U = 1.0\text{eV}$  and  $J_H = U/4$ . (a) FRG flow of  $1/S_{SC,SDW}$ , the inverse of the leading attractive interactions, versus the running energy scale  $\Lambda$ . Notice that  $1/S_{SC,SDW} \rightarrow 0^-$  if  $S_{SC,SDW}$  diverges. The inset shows  $S_{SDW}(\mathbf{q})$  in the unfolded Brillouin zone at the final energy scale. (b) Fermi surface and gap function  $\Delta(\mathbf{k})$  (color scale).

roughly scales with the  $d_{3z^2-r^2}$ -weight of the normal state on this pocket. This is also the case on the  $\delta$  pockets. More interestingly, the gap function on the  $\beta$  pockets diminishes, which is consistent with the frustration caused by the spin scattering between  $\beta$  pockets that would favor  $d_{x^2-y^2}$ -wave pairing instead. Therefore, we obtained a strongly orbital-selective pairing, and the active orbital is  $d_{3z^2-r^2}$ . We notice that similar octet-wise gap minima appears in heavily hole doped  $\text{Ba}_{1-x}\text{K}_x\text{Fe}_2\text{As}_2$ .<sup>50–52</sup> We also notice that the incipient  $s_{\pm}$ -wave is stabilized by the lurking top-flattened  $\gamma$  pocket, which enhances the virtual scattering between  $\alpha$  and  $\gamma$  pockets down to moderate energy scales.

However, with further electron doping, the  $\gamma$  pocket sinks further below the Fermi level, and the effect of  $\alpha$ - $\gamma$  scattering eventually becomes weaker than that between the  $\beta$  pockets. As a result,  $d_{x^2-y^2}$ -wave pairing on the  $\beta$  pockets begin to dominate, as seen in Fig.4 for band filling  $n = 4.35$ . We find that the SDW channel is similar to the case for  $n = 4.24$ , but in the SC channel, the interaction is strong in the incipient  $s_{\pm}$ -wave eigen mode at high energy scales, but the  $d_{x^2-y^2}$ -wave becomes dominant at lower energy scales. The level crossing is indicated by the arrow in Fig.4(a). Fig.4(b) shows the gap function in the band basis, with obvious  $d_{x^2-y^2}$ -wave symmetry. From the gap amplitude distribution, we see the active orbital for this pairing state is  $d_{xy}$  since the gap function vanishes where the  $d_{xy}$  weight of the normal state [as shown in Fig.2(d)] is small. More orbital-resolved details of the pairing form factor can be found in the Appendix A, which may be helpful in orbital-based mean field calculations.

We have performed systematic calculations for various band fillings around  $n = 4$ . Fig.5(a) shows the critical energy scale  $\Lambda_c$  as a function of band filling. We find that the parent compound LaOCrAs has a G-type AFM order, which is consistent with the powder neutron diffraction.<sup>35</sup> With the increase of electron-doping, the

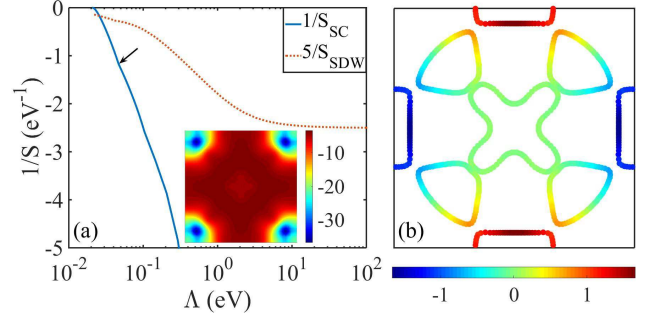


FIG. 4: (Color online) The same plot as Fig.3 but for  $n = 4.35$ . The arrow in (a) indicates the level crossing of the leading pairing channel.

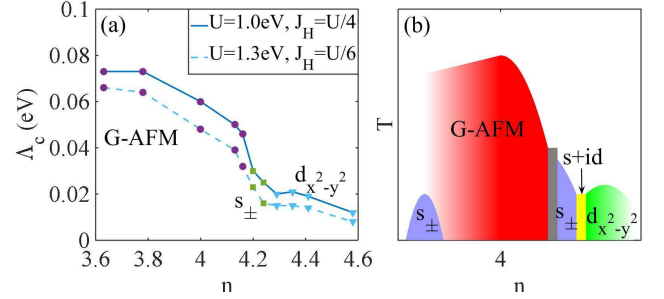


FIG. 5: (Color online)(a) The FRG diverging energy scale  $\Lambda_c$  plotted as a function of band filling. The circles, squares, and triangles represent  $\Lambda_c$  associated with the G-type AFM, incipient  $s_{\pm}$ -wave pairing, and  $d_{x^2-y^2}$ -wave pairing states, respectively.  $U = 1\text{eV}$ ,  $J_H = U/4$  and  $U = 1.3\text{eV}$ ,  $J_H = U/6$  for solid and dashed lines, respectively. (b) A schematic temperature-doping phase diagram for doped LaOCrAs. The gray region denote the transition between G-type AFM state and incipient  $s_{\pm}$ -wave SC state. The dome in the hole doped case indicates the possible  $s_{\pm}$ -wave SC state.

G-type AFM state is suppressed, and the system develops incipient  $s_{\pm}$ -wave SC as the band filling is above 4.2 electrons per site. Upon further electron doping, the system enters the  $d_{x^2-y^2}$ -wave SC state. We also checked the hole-doped case to find that the G-type AFM states are more robust (under the same interactions). This is due to the enhancement from scattering between  $\alpha$  and  $\delta$  pockets, and between the flat bands near Fermi level around  $\Gamma$  and  $M$  points. The above results are not changed qualitatively for  $J_H \in [1/6, 1/4]U$  and moderate  $U$ . As a typical example, we set  $U = 1.3\text{eV}$ ,  $J_H = U/6$ , and perform the FRG calculations. We find that the results are qualitatively the same as the cases with  $U = 1\text{eV}$ ,  $J_H = U/4$ .

We end by presenting a schematic phase diagram for LaOCrAs in the temperature-doping plane in Fig.5(b). There are two domes of superconductivity in electron doped LaOCrAs. With the increase of electron doping, the G-type AFM state gives way to the incipient  $s_{\pm}$ -wave SC state, and subsequently to the  $d_{x^2-y^2}$ -wave SC state. This is somehow similar to the two domes of



superconductivity in electron-doped LaOFeAs with  $H^-$  substitution of  $O^{2-}$ .<sup>53</sup> In the intervening regime between the two domes, the two SC states may become nearly degenerate, and we anticipate a time-reversal-symmetry breaking  $s + id$ -wave SC state is energetically favorable, since the gap function would be maximally open on all fermi pockets. To check this, we perform mean-field calculations to find that  $s + id$ -wave SC state is indeed the ground state between the two domes. (See Appendix B for details.) Finally, in the hole-doped side, we find the  $s_{\pm}$ -wave SC may replace the AFM state if the bare interaction is reduced to  $U = 0.7\text{eV}$ ,  $J_H = U/4$  (or  $U = 0.9\text{eV}$ ,  $J_H = U/6$ ). Following the argument that the effective bare interaction may be reduced significantly far from the Mott limit with  $n = 5$ ,<sup>24,54</sup> we propose that the hole doped LaOCrAs may support  $s_{\pm}$ -wave superconductivity.

#### IV. SUMMARY

We constructed an effective five-band model for Cr  $3d$  orbitals, and investigated possible correlation-driven superconductivity in doped LaOCrAs. With increasing electron doping, we find G-type AFM, incipient  $s_{\pm}$ -wave SC and  $d_{x^2-y^2}$ -wave SC states. The gap function is highly anisotropic on the Fermi surface and highly orbital-selective. Inbetween the two SC phases a time-reversal-symmetry breaking  $s + id$  SC phase is likely to occur. We also propose that the hole-doped LaOCrAs may support the  $s$ -wave SC state.

We notice that superconductivity has not yet been observed experimentally after electron doping in LaOCrAs through  $F^-$  substitution of  $O^{2-}$  with band filling up to  $n = 4.2$ .<sup>35</sup> This is however consistent with our results, since the superconductivity phase appears at  $n > 4.2$  in our phase diagram. Therefore we propose further electron doping in experiment. For this purpose, substitution of  $H^-$  in place of  $O^{2-}$  deserves attention. This type of doping succeeds in iron oxyphnctides in covering a very wide doping range containing two SC domes.<sup>53,55,56</sup> Pressure may further help bring about superconductivity near the band filling 4.2.

#### Acknowledgments

The project was supported by NSFC (under grant Nos.11604168, 11574134, 11404383 and 11604303) and the Ministry of Science and Technology of China (under grant No. 2016YFA0300401). WSW also acknowledges the supports by Zhejiang Open Foundation of the Most Important Subjects (under grant No. xkzwl1613) and K. C. Wong Magna Fund in Ningbo University.

#### Appendix A: Form factors and gap function in the band basis

In this appendix we give the expressions of the form factors, or pairing matrix,  $\phi_{SC}(\mathbf{k})$  in the orbital basis. To describe the momentum dependence, we introduce the lattice harmonics

$$\begin{aligned} c_x &= \cos \mathbf{k}_x, c_y = \cos \mathbf{k}_y; \\ s_x &= \sin \mathbf{k}_x, s_y = \sin \mathbf{k}_y. \end{aligned} \quad (\text{A1})$$

The non-vanishing elements of  $\phi_{SC}(\mathbf{k})$  for  $s_{\pm}$ -wave pairing with band filling  $n = 4.24$  are given by:

$$\begin{aligned} \phi_{SC}^{11}(\mathbf{k}) &= 0.13 + 0.95(c_x + c_y) + 0.44c_xc_y, \\ \phi_{SC}^{22}(\mathbf{k}) &= -0.05 + 0.06c_x + 0.05c_y - 0.02c_xc_y, \\ \phi_{SC}^{33}(\mathbf{k}) &= -0.05 + 0.05c_x + 0.06c_y - 0.02c_xc_y, \\ \phi_{SC}^{44}(\mathbf{k}) &= -0.07 + 0.02(c_x + c_y) - 0.01c_xc_y, \\ \phi_{SC}^{55}(\mathbf{k}) &= -0.03 + 0.03(c_x + c_y) - 0.04c_xc_y, \\ \phi_{SC}^{12}(\mathbf{k}) &= -\phi_{SC}^{21}(\mathbf{k}) = 0.05is_x + 0.11is_xc_y, \\ \phi_{SC}^{13}(\mathbf{k}) &= -\phi_{SC}^{31}(\mathbf{k}) = 0.05is_y + 0.11ic_xs_y, \\ \phi_{SC}^{14}(\mathbf{k}) &= \phi_{SC}^{41}(\mathbf{k}) = -0.02(c_x - c_y), \\ \phi_{SC}^{23}(\mathbf{k}) &= \phi_{SC}^{32}(\mathbf{k}) = 0.01c_xc_y, \\ \phi_{SC}^{24}(\mathbf{k}) &= -\phi_{SC}^{42}(\mathbf{k}) = -0.01is_x, \\ \phi_{SC}^{34}(\mathbf{k}) &= -\phi_{SC}^{43}(\mathbf{k}) = 0.01is_y, \\ \phi_{SC}^{25}(\mathbf{k}) &= -\phi_{SC}^{52}(\mathbf{k}) = 0.01is_y - 0.03ic_xs_y, \\ \phi_{SC}^{35}(\mathbf{k}) &= -\phi_{SC}^{53}(\mathbf{k}) = 0.01is_x - 0.03is_xc_y. \end{aligned} \quad (\text{A2})$$

The non-vanishing elements of  $\phi_{SC}(\mathbf{k})$  for  $d_{x^2-y^2}$ -wave pairing with band filling  $n = 4.35$  are given by:

$$\begin{aligned} \phi_{SC}^{11}(\mathbf{k}) &= 0.02(c_x - c_y), \\ \phi_{SC}^{22}(\mathbf{k}) &= 0.17 + 0.10c_x - 0.01c_xc_y, \\ \phi_{SC}^{33}(\mathbf{k}) &= -0.17 - 0.10c_y + 0.01c_xc_y, \\ \phi_{SC}^{44}(\mathbf{k}) &= 0.03(c_x - c_y), \\ \phi_{SC}^{55}(\mathbf{k}) &= 0.85(c_x - c_y), \\ \phi_{SC}^{12}(\mathbf{k}) &= -\phi_{SC}^{21}(\mathbf{k}) = -0.04is_x + 0.02is_xc_y, \\ \phi_{SC}^{13}(\mathbf{k}) &= -\phi_{SC}^{31}(\mathbf{k}) = 0.04is_y - 0.02ic_xs_y, \\ \phi_{SC}^{14}(\mathbf{k}) &= \phi_{SC}^{41}(\mathbf{k}) = 0.07 + 0.01(c_x + c_y) - 0.01c_xc_y, \\ \phi_{SC}^{24}(\mathbf{k}) &= -\phi_{SC}^{42}(\mathbf{k}) = 0.01is_x, \\ \phi_{SC}^{34}(\mathbf{k}) &= -\phi_{SC}^{43}(\mathbf{k}) = 0.01is_y, \\ \phi_{SC}^{25}(\mathbf{k}) &= -\phi_{SC}^{52}(\mathbf{k}) = -0.28is_y - 0.17ic_xs_y, \\ \phi_{SC}^{35}(\mathbf{k}) &= -\phi_{SC}^{53}(\mathbf{k}) = 0.28is_x + 0.17is_xc_y, \\ \phi_{SC}^{45}(\mathbf{k}) &= \phi_{SC}^{54}(\mathbf{k}) = -0.09s_xs_y. \end{aligned} \quad (\text{A3})$$

With the pairing matrix  $\phi_{SC}$  in the orbital basis, the gap function in the band basis is given by  $\Delta_{\mathbf{k}n} = \langle \mathbf{k}n | \phi_{SC}(\mathbf{k}) | \mathbf{k}n \rangle$  where  $n$  is the band label and  $|\mathbf{k}n\rangle$  is the Bloch state in the given band. Here we used the fact that the normal-state hamiltonian is time-reversal-invariant.

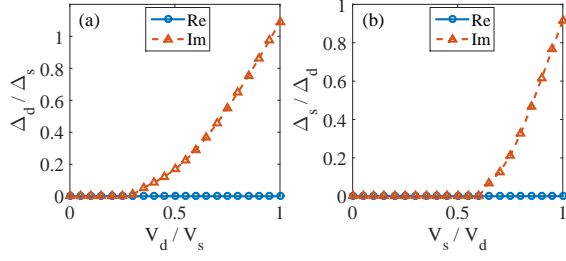


FIG. 6: (Color online)(a)  $\Delta_d/\Delta_s$  versus  $V_d/V_s$  with fixed  $V_s = -0.3\text{eV}$ . The solid and dashed lines are for the real and image parts of  $\Delta_d/\Delta_s$ . (b)  $\Delta_s/\Delta_d$  versus  $V_s/V_d$  with fixed  $V_d = -0.3\text{eV}$ .

### Appendix B: Mean field calculations in the superconducting phase

If both the  $s_{\pm}$ -wave and  $d_{x^2-y^2}$ -wave states are dominant, the effective low-energy Hamiltonian is given by

$$H = H_0 + \frac{V_s}{N} \sum_{\mathbf{k}, \mathbf{k}'} B_{s, \mathbf{k}}^\dagger B_{s, \mathbf{k}'} + \frac{V_d}{N} \sum_{\mathbf{k}, \mathbf{k}'} B_{d, \mathbf{k}}^\dagger B_{d, \mathbf{k}'}, \quad (\text{B1})$$

where  $H_0$  is the normal state dispersion, and  $V_{s/d} < 0$  are the pairing interactions for  $s_{\pm}$ -wave and  $d_{x^2-y^2}$ -wave pairing, respectively.  $N$  is the number of lattice sites, and  $B_{s/d, \mathbf{k}}^\dagger$  are the pairing operator

$$B_{s/d, \mathbf{k}}^\dagger = \Psi_{\mathbf{k}\uparrow}^\dagger \phi_{SC}^{s/d}(\mathbf{k}) (\Psi_{-\mathbf{k}\downarrow}^\dagger)^T, \quad (\text{B2})$$

where  $\Psi_{\mathbf{k}\sigma}^\dagger$  is a spinor creation field for all orbital degrees of freedom and  $\sigma = \uparrow, \downarrow$ . Since the form factor of a given symmetry changes slowly versus the doping level, we use the form factors  $\phi_{SC}^{s/d}(\mathbf{k})$  given in Appendix A for simplicity. The mean-field Hamiltonian can be written as

$$H_{MF} = H_0 + \sum_{\mathbf{k}} [(\Delta_s B_{s, \mathbf{k}}^\dagger + \Delta_d B_{d, \mathbf{k}}^\dagger + \text{h.c.})], \quad (\text{B3})$$

subject to the self-consistent conditions

$$\Delta_{s/d} = \frac{V_{s/d}}{N} \sum_{\mathbf{k}} \langle B_{s/d, \mathbf{k}} \rangle. \quad (\text{B4})$$

In the calculations at zero temperature, out of  $V_s$  and  $V_d$ , we fix one of them so that the mean field  $T_c$  is of the same order of the FRG divergence scale in the corresponding phase, and take the other as a parameter for illustration. We present  $\Delta_d/\Delta_s$  versus  $V_d/V_s$  with fixed  $V_s = -0.3\text{eV}$  in Fig.6(a), and  $\Delta_s/\Delta_d$  versus  $V_s/V_d$  with fixed  $V_d = -0.3\text{eV}$  in Fig.6(b). It is clear that around  $V_s = V_d$  the system develops time-reversal breaking  $s + id$ -wave SC state. Notice that because of different rates of flow, a comparable  $V_s$  and  $V_d$  occurs in FRG only between the two superconducting domes discussed in the main text.

\* Electronic address: wangwansheng@nbu.edu.cn

† Electronic address: qhwang@nju.edu.cn

- <sup>1</sup> Y. Kamihara, T. Watanabe, M. Hirano, and H. Hosono, J. Am. Chem. Soc. **130**, 3296 (2008).
- <sup>2</sup> T. Watanabe, H. Yanagi, T. Kamiya, Y. Kamihara, H. Hiramatsu, M. Hirano, and H. Hosono, Inorg. Chem. **46**, 7719 (2007).
- <sup>3</sup> T. Watanabe, H. Yanagi, Y. Kamihara, T. Kamiya, M. Hirano, and H. Hosono, J. Solid State Chem. **181**, 2117 (2008).
- <sup>4</sup> E. D. Bauer, F. Ronning, B. L. Scott, and J. D. Thompson, Phys. Rev. B **78**, 172504 (2008).
- <sup>5</sup> F. Ronning, N. Kurita, E. D. Bauer, B. L. Scott, T. Park, T. Klimczuk, R. Movshovich, and J. D. Thompson, J. Phys.-Condens. Mat. **20**, 342203 (2008).
- <sup>6</sup> F. Ronning, E. D. Bauer, T. Park, S.-H. Baek, H. Sakai, and J. D. Thompson, Phys. Rev. B **79**, 134507 (2009).
- <sup>7</sup> Y. Tomioka, S. Ishida, M. Nakajima, T. Ito, H. Kito, A. Iyo, H. Eisaki, and S. Uchida, Phys. Rev. B **79**, 132506 (2009).
- <sup>8</sup> D. Hirai, T. Takayama, R. Higashinaka, H. A. Katori, and H. Takagi, J. Phys. Soc. Jpn. **78**, 023706 (2009).
- <sup>9</sup> N. Berry, C. Capan, G. Seyfarth, A. D. Bianchi, J. Ziller, and Z. Fisk, Phys. Rev. B **79**, 180502(R) (2009).
- <sup>10</sup> D. Hirai, T. Takayama, D. Hashizume, R. Higashinaka, A. Yamamoto, A. Hiroko, and H. Takagi, Physica C: Super-

cond. **470**, S296 (2010).

- <sup>11</sup> V. K. Anand, H. Kim, M. A. Tanatar, R. Prozorov, and D. C. Johnston, Phys. Rev. B **87**, 224510 (2013).
- <sup>12</sup> Q. Guo, J. Yu, B. B. Ruan, D. Y. Chen, X. C. Wang, Q. G. Mu, B. J. Pan, G. F. Chen, Z. A. Ren, EuroPhys. Lett. **113**, 17002 (2016).
- <sup>13</sup> K. Kudo, Y. Nishikubo, and M. Nohara, J. Phys. Soc. Jpn. **79**, 123710 (2010).
- <sup>14</sup> M. Imai, S. Emura, M. Nishio, Y. Matsushita, S. Ibuka, N. Eguchi, F. Ishikawa, Y. Yamada, T. Muranaka, and J. Akimitsu, Supercond. Sci. Technol. **26**, 075001 (2013).
- <sup>15</sup> Y. Singh, A. Ellern, and D. C. Johnston, Phys. Rev. B **79**, 094519 (2009).
- <sup>16</sup> Y. Singh, M. A. Green, Q. Huang, A. Kreyssig, R. J. McQueeney, D. C. Johnston, and A. I. Goldman, Phys. Rev. B **80**, 100403 (2009).
- <sup>17</sup> R. Nath, V. O. Garlea, A. I. Goldman, and D. C. Johnston, Phys. Rev. B **81**, 224513 (2010).
- <sup>18</sup> N. Emery, E. J. Wildman, J. M. S. Skakle, A. C. McLaughlin, R. I. Smith, and A. N. Fitch, Phys. Rev. B **83**, 144429 (2011).
- <sup>19</sup> A. T. Satya, A. Mani, A. Arulraj, N. V. Chandra Shekar, K. Vinod, C. S. Sundar, and A. Bharathi, Phys. Rev. B **84**, 180515 (2011).
- <sup>20</sup> Abhishek Pandey, R. S. Dhaka, J. Lamsal, Y. Lee, V. K. Anand, A. Kreyssig, T. W. Heitmann, R. J. McQueeney,

- A. I. Goldman, B. N. Harmon, A. Kaminski, and D. C. Johnston Phys. Rev. Lett. **108**, 087005 (2012).
- <sup>21</sup> J. Lamsal, G. S. Tucker, T. W. Heitmann, A. Kreyssig, A. Jesche, A. Pandey, W. Tian, R. J. McQueeney, D. C. Johnston, and A. I. Goldman, Phys. Rev. B **87**, 144418 (2013).
  - <sup>22</sup> J. Guo, J. Simonson, L. Sun, Q. Wu, P. Gao, C. Zhang, D. Gu, G. Kotliar, M. Aronson, and Z. Zhao, Sci. Reports **3**, 2555 (2013).
  - <sup>23</sup> T. Hanna, S. Matsuishi, K. Kodama, T. Otomo, S. I. Shamoto, and H. Hosono, Phys. Rev. B **87**, 020401(R) (2013).
  - <sup>24</sup> J. M. Pizarro, M. J. Calderón, J. Liu, M. C. Muñoz, and E. Bascones, arXiv: 1610.09560.
  - <sup>25</sup> M. Edelmann, G. Sangiovanni, M. Capone, and L. de' Medici, arXiv: 1610.10054.
  - <sup>26</sup> W. Wu, J. Cheng, K. Matsubayashi, P. Kong, F. Lin, C. Jin, N. Wang, Y. Uwatoko, and J. Luo, Nat. Commun. **5**, 5508 (2014).
  - <sup>27</sup> H. Kotegawa, S. Nakahara, H. Tou, and H. Sugawara, J. Phys. Soc. Jpn. **83**, 093702 (2014).
  - <sup>28</sup> J. K. Bao, J. Y. Liu, C. W. Ma, Z. H. Meng, Z. T. Tang, Y. L. Sun, H. F. Zhai, H. Jiang, H. Bai, C. M. Feng, Z. A. Xu, and G. H. Cao, Phys. Rev. X **5**, 011013 (2015).
  - <sup>29</sup> Z. T. Tang, J. K. Bao, Y. Liu, Y. L. Sun, A. Ablimit, H. F. Zhai, H. Jiang, C. M. Feng, Z. A. Xu, and G. H. Cao, Phys. Rev. B **91**, 020506 (2015).
  - <sup>30</sup> Z. T. Tang, J. K. Bao, Z. Wang, H. Bai, H. Jiang, Y. Liu, H. F. Zhai, C. M. Feng, Z. A. Xu, and G. H. Cao, Sci. Chin. Mater. **58**, 16 (2015).
  - <sup>31</sup> M. Pfisterer and G. Nagorsen, Z. Naturforsch. B **35**, 703 (1980).
  - <sup>32</sup> D. J. Singh, A. S. Sefat, M. A. McGuire, B. C. Sales, D. Mandrus, L. H. VanBebber, and V. Keppens, Phys. Rev. B **79**, 094429 (2009).
  - <sup>33</sup> M. Rotter, M. Tegel, and D. Johrendt, Phys. Rev. Lett. **101**, 107006 (2008).
  - <sup>34</sup> U. B. Paramanik, R. Prasad, C. Geibel, and Z. Hossain, Phys. Rev. B **89**, 144423 (2014).
  - <sup>35</sup> S. W. Park, H. Mizoguchi, K. Kodama, S. i. Shamoto, T. Otomo, S. Matsuichi, T. Kamiya, and H. Hosono, Inorg. Chem. **52**, 13363 (2013).
  - <sup>36</sup> H. Jiang, J. K. Bao, H. F. Zhai, Z. T. Tang, Y. L. Sun, Y. Liu, Z. C. Wang, H. Bai, Z. A. Xu, and G. H. Cao, Phys. Rev. B **92**, 205107 (2015).
  - <sup>37</sup> W.-S. Wang, Y.-Y. Xiang, Q.-H. Wang, F. Wang, F. Yang, and D.-H. Lee, Phys. Rev. B **85**, 035414 (2012).
  - <sup>38</sup> Y.-Y. Xiang, W.-S. Wang, Q.-H. Wang, and D.-H. Lee, Phys. Rev. B **86**, 024523 (2012).
  - <sup>39</sup> Y.-Y. Xiang, F. Wang, D. Wang, Q.-H. Wang, and D.-H. Lee, Phys. Rev. B **86**, 134508 (2012).
  - <sup>40</sup> W.-S. Wang, Z.-Z. Li, Y.-Y. Xiang, and Q.-H. Wang, Phys. Rev. B **87**, 115135 (2013).
  - <sup>41</sup> Y.-Y. Xiang, Y. Yang, W.-S. Wang, Z.-Z. Li, Q.-H. Wang, Phys. Rev. B **88**, 104516 (2013).
  - <sup>42</sup> Y. Yang, W.-S. Wang, Y.-Y. Xiang, Z.-Z. Li, Q.-H. Wang, Phys. Rev. B **88**, 094519 (2013).
  - <sup>43</sup> Q. H. Wang, C. Platt, Y. Yang, C. Honerkamp, F. C. Zhang, W. Hanke, T. M. Rice, R. Thomale, Europhys. Lett. **104**, 17013 (2013).
  - <sup>44</sup> Y. Yang, W.-S. Wang, J.-G. Liu, H. Chen, J.-H. Dai and Q.-H. Wang, Phys. Rev. B **89**, 094518 (2014).
  - <sup>45</sup> W.-S. Wang, Y. Yang, Q. H. Wang, Phys. Rev. B **90**, 094514 (2014).
  - <sup>46</sup> P. Giannozzi, *et al.*, J.Phys.:Condens.Matter, **21**, 395502 (2009); <http://www.quantum-espresso.org>; Here we adopt the exchange correlation functional introduced by J. P. Perdew, K. Burke and M. Ernzerhof [Phys. Rev. Lett. **77**, 3865 (1996)], and the wave functions are expanded by plane waves up to a cutoff energy of 45 Ry. Also,  $20 \times 20 \times 10$  **k**-point meshes are used with the special points technique by H. J. Monkhorst and J. D. Pack [Phys. Rev. B **13**, 5188 (1976)]. The high-throughput ultrasoft pseudopotentials given in GBRV database are used in our first-principles calculation [K. F. Garrity, J. W. Bennett, K. M. Rabe and D. Vanderbilt, Comput. Mater. Sci. **81**, 446 (2014)].
  - <sup>47</sup> N. Marzari and D. Vanderbilt, Phys. Rev. B **56**, 12847 (1997); I. Souza, N. Marzari, and D. Vanderbilt, *ibid.* **65**, 035109 (2001); A. A. Mostofi, J. R. Yates, G. Pizzi, Y. S. Lee, I. Souza, D. Vanderbilt, and N. Marzari, Comput. Phys. Commun. **185**, 2309(2014); The Wannier functions are generated by the code developed by A. A. Mostofi, J. R. Yates, N. Marzari, I. Souza, and D. Vanderbilt, <http://www.wannier.org/>.
  - <sup>48</sup> The main scheme is the same as K. Kuroki, S. Onari, R. Arita, H. Usui, Y. Tanaka, H. Kontani, and H. Aoki, Phys. Rev. Lett. **101**, 087004 (2008).
  - <sup>49</sup> Notice that upon point group operations the orbitals also change. See, e.g., Y. Wan and Q. H. Wang, Europhys. Lett. **85**, 57007 (2009).
  - <sup>50</sup> K. Okazaki, Y. Ota, Y. Kotani, W. Malaeb, Y. Ishida, T. Shimojima, T. Kiss, S. Watanabe, C.-T. Chen, K. Kihou, C. H. Lee, A. Iyo, H. Eisaki, T. Saito, H. Fukazawa, Y. Kohori, K. Hashimoto, T. Shibauchi, Y. Matsuda, H. Ikeda, H. Miyahara, R. Arita, A. Chainani, and S. Shin, Science **337**, 1314 (2012).
  - <sup>51</sup> Y. Ota, K. Okazaki, Y. Kotani, T. Shimojima, W. Malaeb, S. Watanabe, C.-T. Chen, K. Kihou, C. H. Lee, A. Iyo, H. Eisaki, T. Saito, H. Fukazawa, Y. Kohori, and S. Shin, Phys. Rev. B **89**, 081103(R) (2014).
  - <sup>52</sup> N. Xu, P. Richard, X. Shi, A. van Roekeghem, T. Qian, E. Razzoli, E. Rienks, G.-F. Chen, E. Ieki, K. Nakayama, T. Sato, T. Takahashi, M. Shi, and H. Ding, Phys. Rev. B **88**, 220508(R) (2013).
  - <sup>53</sup> S. Iimura, S. Matsuichi, H. Sato, T. Hanna, Y. Muraba, S. W. Kim, J. E. Kim, M. Takata, and H. Hosono, Nat. Commun. **3**, 943 (2012).
  - <sup>54</sup> H. Ishida and A. Liebsch, Phys. Rev. B **81**, 054513 (2010).
  - <sup>55</sup> S. Matsuishi, T. Hanna, Y. Muraba, S. W. Kim, J. E. Kim, M. Takata, S. I. Shamoto, R. I. Smith, and H. Hosono, Phys. Rev. B **85**, 014514 (2012).
  - <sup>56</sup> S. Matsuishi, T. Maruyama, S. Iimura, H. Hosono, Phys. Rev. B **89**, 094510 (2014).